Biosensors and Bioelectronics 145 (2019) 111563

Contents lists available at ScienceDirect

Biosensors and Bioelectronics

journal homepage: www.elsevier.com/locate/bios

# Ultrasensitive biosensor based on magnetic microspheres enhanced microfiber interferometer

Rahul Kumar[a,b,1], Yuankui Leng[c,1], Bin Liu[a,1], Jun Zhou[d], Liyang Shao[e,**], Jinhui Yuan[f], Xinyu Fan[g,***], Shengpeng Wan[a], Tao Wu[a], Juan Liu[a], Richard Binns[b], Yong Qing Fu[b], Wai Pang Ng[b], Gerald Farrell[h], Yuliya Semenova[h], Hengyi Xu[c], Yonghua Xiong[c], Xingdao He[a,****], Qiang Wu[a,b,*]

[a] National Engineering Laboratory for Destructive Testing and Optoelectronic Sensing Technology and Application, Nanchang HangKong University, Nanchang, 330063, China
[b] Faculty of Engineering and Environment, Northumbria University, Newcastle Upon Tyne, NE1 8ST, United Kingdom
[c] Nanchang University, State Key Lab Food Sci & Technol, 235 Nanjing East Rd, Nanchang, 330047, Jiangxi, PR China
[d] Faculty of Science, Institute of Photonics, Ningbo University, Ningbo, 315211, Zhejiang, China
[e] Department of Electrical and Electronic Engineering, Southern University of Science and Technology of China, Shenzhen, PR China
[f] State Key Laboratory of Information Photonics and Optical Communications, Beijing University of Posts and Telecommunications, Beijing, China
[g] State Key Lab Adv Opt Commun Syst & Networks, Shanghai Jiao Tong University, 800 Dongchuan Rd, Shanghai, 200240, PR China
[h] Photonics Research Centre, Technological University Dublin, Ireland

ARTICLE INFO

*Keywords:*
Biosensor
Human chorionic gonadotropin (hCG)
Optical fiber sensor
Optical fiber interferometer

ABSTRACT

A critical barrier for the successful development of fiber sensors for bio-chemical processes is their limitedly improved sensitivity, restricted by the sensor structural design. To solve this, in this paper, a novel concept was proposed using functionalised modified magnetic microspheres (MMSs) to "amplify" the effect of target bio-chemical analytes to significantly improve the fiber sensor's sensitivity, which has been demonstrated using human chorionic gonadotropin (hCG) as an example. Two types of antibody hCG, (***β*** and ***α***, both can specifically bind with hCG), were adhered on the surface of fibre sensor and MMSs respectively. Both hCG and MMSs will be specifically captured by the fibre sensor, where MMSs act as an "amplifier" to improve the sensor sensitivity. Experimentally immunomagnetic detection limit of 0.0001 mIU/mL has been achieved, which is the highest reported so far. This newly developed methodology opens a new direction for sensitivity improvement and could be further explored to applications require ultrahigh sensitivity detections such as earlier medical diagnostics.

## 1. Introduction

Human chorionic gonadotropin (hCG) is a glycoprotein secreted by placental trophoblast cell after implantation. It simulates the corpus luteum in the ovary to produce progesterone, which maintains the lining of the uterus during the first week of pregnancy (Noonan et al., 1979). hCG is a heterodimer composed of two different α- and β-subunits combined by noncovalent bonds, where β subunit is the most important diagnostic markers for pregnancy and tumor, due to it being unique to hCG, while the α-subunit is identical to luteinizing hormone, follicle-stimulating hormone and thyroid-stimulating hormone (TSH) (Fan et al., 2017). The hCG level in urine sample of pregnant women are an important parameter for determining pregnancy and its related disorder. In practice an hCG level > 5 mIU/mL is considered positive for pregnancy. However, the current pregnancy test strip has a relatively low detection threshold of 10 mIU/mL, which can only be reached after 2 weeks after conception (Malhotra et al., 2015; Pocius et al., 2015, 2017). Elevated levels of hCG have been reported in tumor patients (Sheth et al., 1974; Shah et al., 2008), thus hCG level can also be an indicator of a tumor and measurements of the hCG level are

* Corresponding author. Faculty of Engineering and Environment, Northumbria University, Newcastle Upon Tyne, NE1 8ST, United Kingdom.
** Corresponding author.
*** Corresponding author.
**** Corresponding author.
*E-mail addresses:* shaoly@sustech.edu.cn (L. Shao), fan.xinyu@sjtu.edu.cn (X. Fan), hxd@nchu.edu.cn (X. He), qiang.wu@northumbria.ac.uk (Q. Wu).
[1] These authors have equal contributions to this paper.

https://doi.org/10.1016/j.bios.2019.111563
Received 21 May 2019; Received in revised form 16 July 2019; Accepted 1 August 2019
Available online 06 August 2019
0956-5663/ 

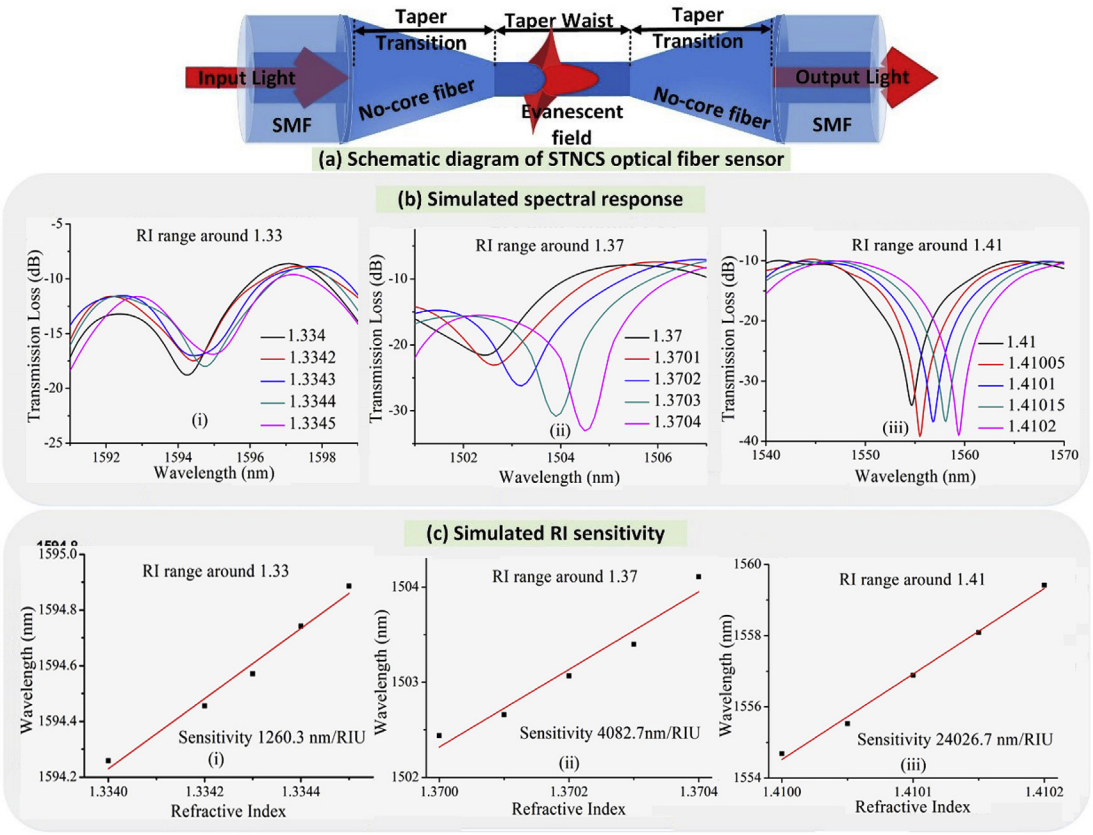


**Fig. 1.** (a) Schematic view of the STNCS optical fiber structure; (b) Simulated spectral response, and (c) RI sensitivity predicted using simulation, for STNCS structure with 8 μm taper waist diameter in different RI ranges of 1.33, 1.37 and 1.41 respectively.

important for monitoring the recovery of patients receiving chemotherapy (Douglas et al., 2014). When the concentration of hCG in serum reaches 15–150 mIU/mL, the diagnosis of a gonadal tumor or testicular seminoma is almost certain (Yan et al., 2012). On the other hand, detection of hCG is important in sports medicine, since its high levels could be linked to cases of concealed use of anabolic steroids aiming to increase the production of testosterone by athletes and is therefore banned by World Anti-doping Agency (Berger and Sturgeon, 2014). Normally hCG concentration in a human body is very low (0.02–0.8 mIU/mL) (Keay et al., 2004) and hence a very high sensitivity hCG sensor is required to detect the concentration of hCG with high resolution and low detection limit.

The current hCG detection techniques utilize immune recognition based on the high binding affinity between hCG-α or -β antibodies (Ab) and the hCG antigen (Ag). This Ab-Ag interaction have led to the development of various immunosensors for hCG detection, such as Enzyme immunosensor (EIS), Electrochemical immunosensor (ECIS) and Photochemical immunosensor (PCIS) which detect the changes in electrical signal, when hCG from the sample binds with the hCG-Ab immobilized on the electrode surface. EIS is one of the earliest methods for determining hCG concentration, which combines the amplification of enzyme-catalyzed reaction with the specificity of Ab-Ag affinity reaction. EIS has relatively low sensitivity of 0.4 mIU/mL and is only suitable for qualitative and semi qualitative determination (Imamura et al., 1976). Santandrew et al. in (Santandreu et al., 1999) proposed an amperometric immunosensor consisting of a conducting graphite-methacrylate matrix functionalized with anti-β-hCG Ab, with a limit of detection (LOD) of 2.6 mIU/mL hCG. The LOD has been improved to as low as 0.00036 mIU/mL (Wang et al., 2010) with the cost of increased complexity of depositing carbon nanotubes film on the electrodes to increase conductivity of such electronic sensors. PCIS is another type of immunosensors used for hCG detection, which require a secondary Ab linked with reagent to produce fluorescence. Since the intensity of fluorescence is normally very weak, this type of sensors often suffers from the background interference (ambient light). An example of PCIS was demonstrated by L. Mao et al. in (Mao et al., 2010) with a low LOD of 0.07 mIU/mL using $TiO_2$ composite nanoparticles functionalized by Nafion as label. Surface plasmon resonance (SPR) based immunosensor are another method for direct and rapid detection of biology samples. A SPR immunosensor with good specificity and selectivity, but relatively low LOD of 100 mIU/mL hCG, was demonstrated by M. Piliarik et al. in (Piliarik et al., 2010).

Due to the advantages of compact size, immunity to electromagnetic interference and remote sensing capabilities (Zhao et al., 2016), optical fiber sensors have attracted wide research interests in many areas such as automotive, chemical industry, aircraft, medical diagnosis, etc. (Hassan et al., 2016). Numerous optical fiber-based sensor structures have been developed as biosensors, such as fiber Bragg gratings (FBGs) (Liu et al., 2018a,b), tapered fibers (Mustapa et al., 2018), fiber interferometers (Sepúlveda et al., 2006; Wang and Wang, 2018), photonics crystal fibers (Betancur-Ochoa et al., 2017), dual core fibers (Wysokiński et al., 2018), etc. Among these optical fiber sensor structures, the interferometric sensors based on a singlemode-multimode-singlemode (SMS) (Wu et al., 2011) fiber structure have unique advantages of simple fabrication process, low cost and high sensitivity and hence have been widely investigated worldwide (Liu et al., 2015, 2018a,b).

In this paper, we propose an ultrasensitive microfiber interferometer biosensor for ultralow hCG concentration detection. The fiber sensor structure used for this study is a singlemode-tapered no-core-singlemode (STNCS) optical fiber sensor, which generates easily accessible evanescent field around its tapered waist region. The fiber sensor is then functionalised by immobilizing anti-hCG-β Ab on the fiber sensor surface, specifically around the waist region and is then

demonstrated to detect hCG in a sample with concentration as low as 0.05 mIU/mL. To further improve the sensitivity of the sensor, MMSs immobilized with anti-hCG-α Ab were added to the hCG analyte, which effectively increases the surrounding refractive index (RI) (because of large size of MMSs) due to the capture of hCG samples. Experimentally, the sensor can detect hCG concentrations < 0.01 mIU/mL by adding surface modified MMS and enriched hCG samples.

## 2. Principle and simulation

A schematic diagram of the microfiber interferometer is shown in Fig. 1 (a). As the input light propagates from the input singlemode fiber (SMF) into the no-core fiber (NCF), multiple modes will be excited and propagate within the NCF section. When the NCF is tapered to small diameters, the percentage of evanescent field transmitted around the NCF surface increases significantly, resulting in the increase of RI sensitivity of the fiber sensor, which is the base for hCG detection in this paper. Fig. 1(b) and (c) shows simulation results for the spectral response and RI sensitivity of the tapered NCF structure, respectively. Since the tapered NCF diameter in the transition region [Fig. 1 (a)] changes continuously, the traditional mode transmission method (Wu et al., 2011) isn't suitable to simulate the RI sensitivity. In this case, beam propagation method (BPM) with 2D model is used to investigate the RI sensitivity of the structure. In the simulation, the RI of tapered no-core fiber is 1.4428 with taper waist of 8 μm, the length of the tapered no-core fiber section is 10 mm and each of the taper transition sections have a length of 7 mm. The SMF has core and cladding diameter of 9 and 125 μm, and the corresponding RI of 1.4507 and 1.4428 respectively. As shown in Fig. 1 (c), as the RI increases, the wavelength shifts to longer wavelength in all the three RI ranges of 1.33, 1.37 and 1.41. The shift rates (slope) of the wavelength shift for the three RI ranges are different, where higher RI range of 1.41 has maximum slope of 24,026.7 nm/Refractive index unit (RIU), showing very high RI sensitivity for this sensor.

## 3. Experimental method

An STNCS optical fiber structure with 8 μm waist diameter is used as a platform for the development of hCG biosensor in our experiments. Before modifying the fiber sensor surface for hCG detection, an RI sensitivity test has been carried out, and the results are shown in Fig. 2(a–c).

As observed in Fig. 2(a–c), the RI sensitivities of the STNCS optical fiber sensor with 8 μm waist diameter are 1046.34, 3780.10 and 26,061.77 nm/RIU for the RI ranges around 1.33, 1.37 and 1.41, respectively, which agrees very well with the simulation results (1260.3, 4082.7 and 24,026.7 nm/RIU for the RI ranges around 1.33, 1.37 and 1.41).

The stability test for the sensor has also been carried out as shown in Fig. 2 (d). In this experiment, phosphate buffer saline (PBS) was used for stability tests which is also used for diluting and washing hCG in the bio-sensing tests at a later stage. As shown in Fig. 2(d), three rounds of stability tests have been carried out and one can see from the figure, the wavelength shift is stable and repeatable with an average spectral variation of ± 0.05 nm over 60 min duration. Fig. 2(d) also shows that the wavelength shift mainly occurred in the first 5 min, which is possibly due to the instability introduced by the initial flow of the PBS liquid in each stability test.

### 3.1. Fiber surface modification and Ab immobilization

The developed STNCS sensor is then functionalized by immobilizing anti-hCG-β Ab as a capture Ab on the fiber sensor surface, to ensure specific binding with hCG. When the hCG binds with anti hCG-β Ab, both effective RI and thickness of the STNCS sensor will change, resulting in the wavelength shift of the sensor.

The schematic fiber surface modification and immobilization procedure is shown in Fig. 3(a) and is as follows (Soteropulos and Hunt, 2012):

i) The fiber surface is treated with 5% silane reagent (3-(Triethoxysilyl)propylsuccinic anhydride) in ethanol for 2–4 h in room temperature to attach carboxyl groups to the fiber surface.
ii) After washing the fiber sensor with ethanol and PB (Phosphate buffer without sodium chloride) buffer (pH = 6.0), the fiber surface is treated with freshly prepared EDC (1-ethyl-3-(-3-dimethylaminopropyl) carbodiimide hydrochloride) and NHS (N-hydroxysuccinimide) solution for 1 h. This step couples an activated succimide ester (obtained from EDC and NHS reaction), to which the capture antibody can easily attach.
iii) The fiber surface is immediately treated with the capture antibody in PBS (Phosphate buffer saline), for 4 h.
iv) After being taken out from the capture antibody in PBS, the fiber sensor is immersed into 1% BSA (Bovine serum albumin) for 2 h at room temperature to block the excess NHS ester and the uncovered gaps of fiber sensor, thus supressing unspecified biofouling.
v) Finally, the fiber sensor is washed with a PBS buffer before using it to detect an hCG sample.

Fig. 3(c) shows a schematic diagram of the experimental setup. The light supplied by a broadband source (SLD1005S) is launched into the functionalised STNCS fiber sensor, which is placed in a microchannel of volume ~ 400 μL, and the output light from the sensor is detected by an optical spectral analyser (OSA, Yokogawa AQ6370D). The microchannel (400 μL) is then filled with samples with different hCG concentrations. The hCG in the sample will be captured by the hCG-β Ab and bind to the fiber sensor surface so that the higher the hCG concentration, the more hCG will be captured, resulting in a larger change of the effective RI and coating thickness. The interaction of evanescent field with the hCG captured by the hCG-β Ab on the fiber surface, which causes change in the RI is illustrated in Fig. 3(b). The capture antibody on the fiber surface selectively binds with the hCG present in the urine sample based on a non-covalent bond, as shown in Fig. 3(d–i). The scanning electron microscope (SEM) images of the (i) STNCS waist cross-section, (ii) modified STNCS fiber after hCG detection and (iii) binding of anti hCG-β Ab modified MMSs (supplied by Ocean nanoTech corporation (USA)) on the fiber surface are shown in Fig. 3(e).

In the hCG detection experiment, six different concentrations of hCG (0.05, 0.5, 5, 50, 500, 500 mIU/mL) are prepared by diluting the stock urine sample (17,857 mIU/mL hCG) in PBS. The spectral response of the fiber sensor to the different concentrations of hCG is observed by adding each of the hCG samples, starting from the lowest (0.05 mIU/mL) to the highest (500 mIU/mL) hCG concentration, in the above concentration series. After each measurement, and before introducing the next concentration of hCG, PBS is added in the channel for 10 min to wash the un-bonded hCG due to gravitational deposition. This washing step is important to eliminate the influence of the un-bonded or loosely bonded hCG.

### 3.2. Preparation of MMS functionalized with anti-hCG-α Ab

Anti-hCG-α antibodies were immobilized on the surface of MMS via amido bond formed between the amino group of antibodies and the carboxyl group of the magnetic beads. Typically for 300 nm MMS, 200 μL of MMS (50 pM) were washed three times with phosphate buffer (PB, 0.01 M, pH = 6.0). Then 100 μL of anti-hCG-α Ab solution (1 mg/mL) was added for a 30 min incubation under gentle shaking at ambient temperature. Thereafter, 50 μL of EDC•HCl solution (1 mg/mL) was added into the mixture, followed by a 30 min incubation under gentle shaking at room temperature. Then 100 μL of BSA solution (1 mg/mL) was added to block the MMS via the same procedure. The resulting anti-hCG-α Ab modified MMS were separated and washed three times with

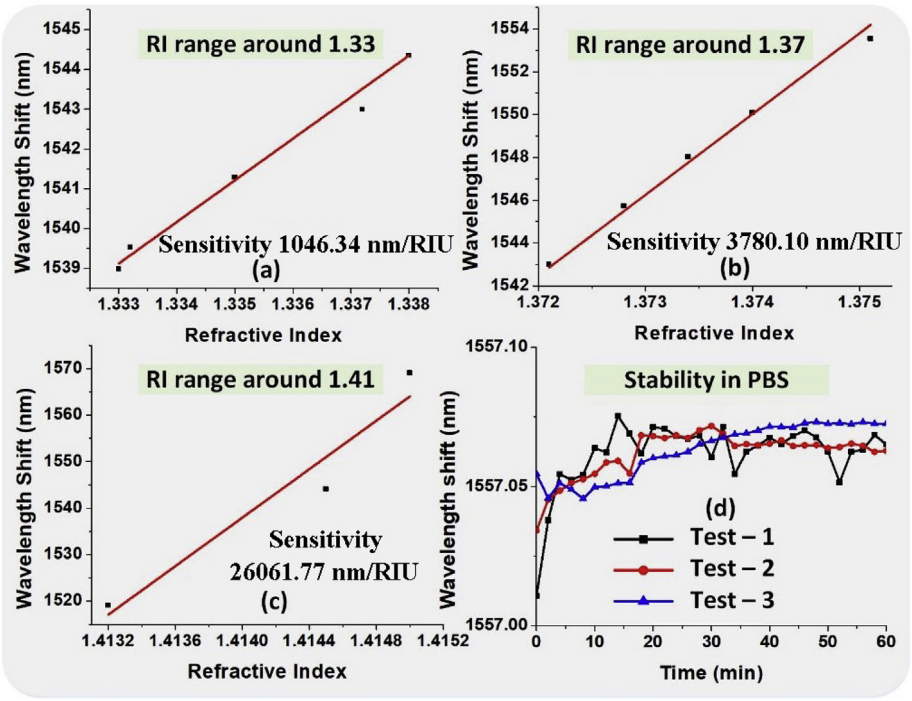


**Fig. 2.** Experimentally observed RI sensitivity of the STNCS optical fiber sensor in different RI ranges: (a) circa 1.33; (b) circa 1.37; (c) ~1.41 and (d) stability of the STNCS in PBS.

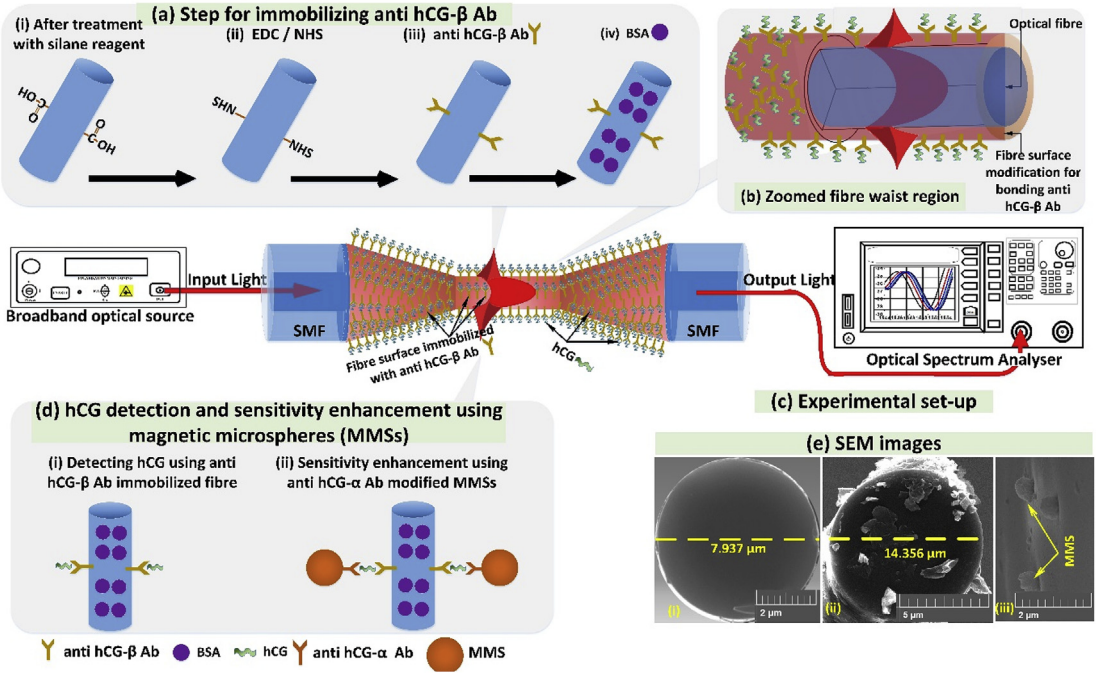


**Fig. 3.** (a) Surface modification and Ab immobilization procedure; (b) Zoomed fiber waist region showing RI change caused by the bonding of hCG on the fiber surface, immobilized with hCG-β Ab; (c) Experimental setup for hCG detection; (d) Functionalised fiber sensor for hCG detection and sensitivity enhancement using MMSs; (e) SEM images for STNCS; (i) waist cross-section, (ii) functionalized fiber after hCG detection and (iii) hCG-α modified MMSs bound to the fiber sensor surface.

PB buffer via magnetic separation.

## 4. Result and discussion

### 4.1. Investigation of capture layer concentration

The influence of capture Ab concentration on the performance of the sensor was firstly studied using four identical STNCS fiber sensors (fabricated under the same conditions) immobilized with four different concentrations (4, 8, 16 and 32 µg/mL) of capture Ab, to detect hCG samples with different concentrations of 0.05, 0.5, 5, 50, 500 mIU/mL respectively. Fig. 4(a) shows an example of the output spectral response of the STNCS fiber sensor immersed in three different concentrations (0.05, 5, and 500 mIU/m L) of hCG, where the fiber sensor surface is

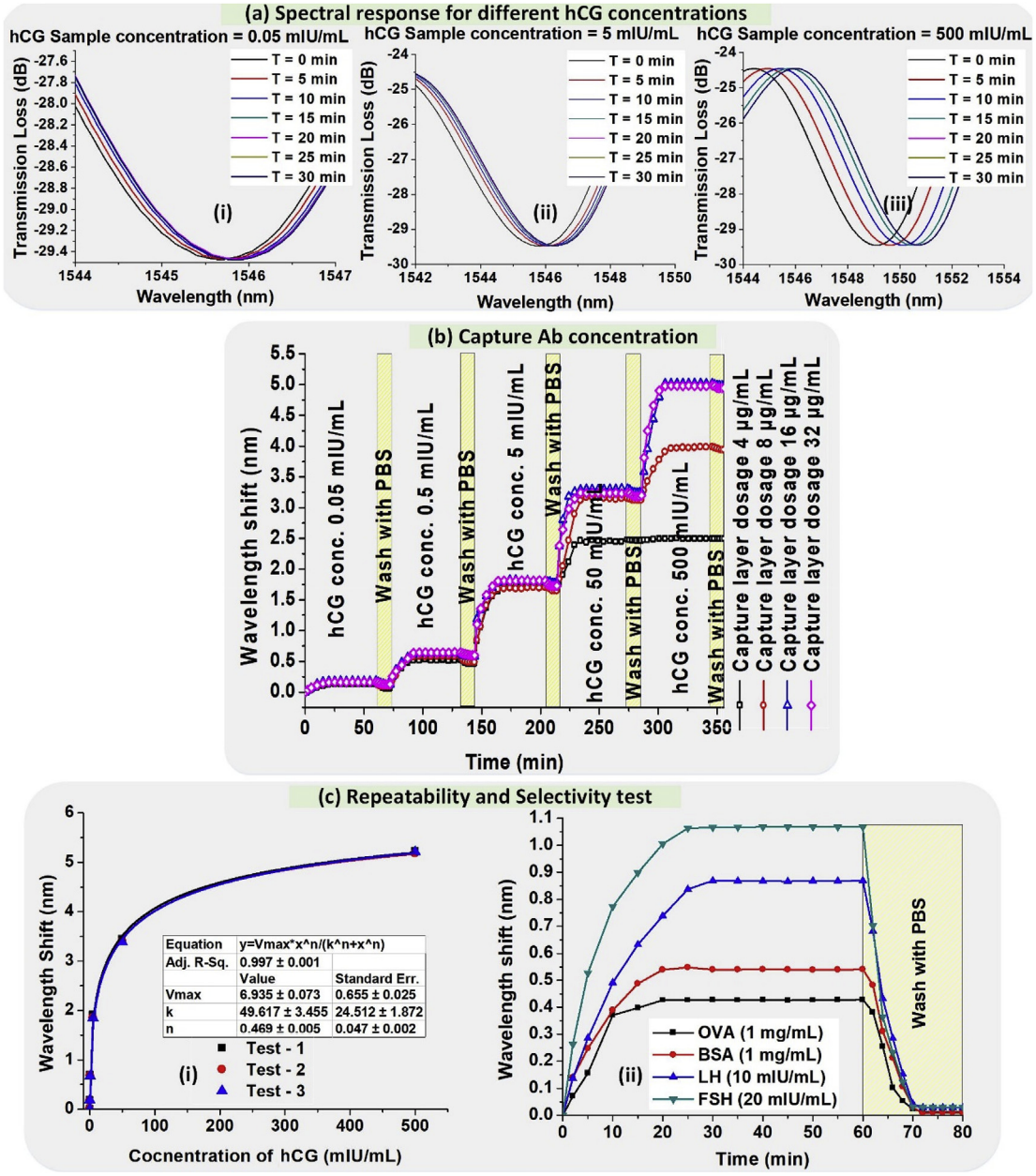


**Fig. 4.** (a) Spectral response of the STNCS fiber sensor functionalised with 16 µg/mL of capture Ab concentration, to detect (i) 0.05 mIU/mL (ii) 5 mIU/mL and (iii) 500 mIU/mL of hCG concentration in urine sample; (b) Investigation of capture Ab concentration on the capability of the STNCS fiber surface to detect hCG in the entire sample range from 0.05 to 500 mIU/mL; (c) (i) Repeatability and (ii) Selectivity test for STNCS optical fiber sensor immobilized with 16 µg/mL of capture Ab.

modified with 16 µg/mL of capture Ab. It can be observed that, as the time of immersion increases, the wavelength dip in the output spectrum of the sensor shifts towards a longer wavelength, which is due to the binding of hCG on to the functionalised fiber surface. The higher the hCG concentration, the larger is the spectral dip shift. It is noted that, the spectral shift is observed mainly in the initial 20 min, after which the spectral response stabilises.

Fig. 4(b) summarizes the wavelength shift vs time for the four functionalised STNCS fiber sensors above at different concentrations of hCG samples (0.05, 0.5, 5, 50, 500, 5000 mIU/mL). It can be seen that, when the hCG concentration is 50 mIU/mL, the capture Ab immobilized with dosage of 4 µg/mL will be saturated, hence not capable to detect hCG with concentrations higher than 50 mIU/mL. If the maximum detectable hCG concentration is less than 500 mIU/mL, the optimum capture Ab dosage for immobilization is 16 µg/mL and the total spectral shift observed is 5.22 nm for hCG concentration of 500 mIU/mL. Increasing the capture Ab dosage to 32 µg/mL does not show any significant improvement to the wavelength shift, with a total spectral shift of 5.18 nm for the same hCG concentration. Therefore, in our further experiments STNCS optical fiber immobilised with 16 µg/mL of capture Ab is used.

The repeatability of the proposed sensor was tested and the result is shown in Fig. 4(c–i). The results show that the sensor has good repeatability with an average wavelength shift of 0.18 ± 0.01, 0.69 ± 0.01, 1.91 ± 0.04, 3.44 ± 0.03, and 5.22 ± 0.02 nm for 0.05, 0.5, 5, 50, 500 mIU/mL of hCG, respectively. Based on these values, a standard curve fitting is achieved as described by Eq. (1). By measuring the wavelength shift $y$, the hCG concentration $x$ can thus be calculated solving Eq. (1):

$$y = \frac{6.884 \times x^{0.471}}{6.047 + x^{0.471}} \quad (1)$$

To test the selectivity of the proposed sensor, four different non-specific analytes (1 mg/mL of ovalbumin (OVA), 1 mg/mL of bovine serum albumin (BSA), 10 mIU/mL of Luteinizing hormone (LH), and 20 mIU/mL of Follicle-stimulating hormone (FSH) were introduced separately to the functionalised fiber sensor and the result is shown in Fig. 4(c–ii). As can be seen in Fig. 4(c–ii), during the initial 25 min, significant dip wavelength shift was observed by around 0.43, 0.54, 0.86 and 1.06 nm for OVA, BSA, LH and FSH, respectively. After 30 min, the reading was stable and the fiber sensor was then washed with PBS for 20 min, where the dip wavelength is observed to shift back to almost the same value of the initial dip wavelength, with only 0.013, 0.010, 0.028, 0.030 nm wavelength deviations for OVA, BSA, LH and FSH, respectively. This result indicates that the fiber sensor has very good selectivity for hCG. The significant dip wavelength shift observed is due to the nonspecific bind or gravitational deposition of high concentration analytes, which can be washed by PBS.

### 4.2. Sensitivity improvement by using functionalized magnetic microspheres (MMSs)

Our initial experiment demonstrated that the sensor can detect hCG with concentration as low as 0.05 mIU/mL, where the sensitivity is as high as 3.76 nm/mIU/mL. To further improve the sensitivity of the fiber sensor, we propose to use MMSs functionalized with anti-hCG-α Ab, which will bind with the analyte hCG captured by the anti-hCG-β Ab on the fiber surface to introduce additional increase in effective RI and thickness of the fiber coating. Fig. 3(d) shows the schematic diagram of the scheme by adding additional MMSs functionalized with anti-hCG-α Ab to the sensing system. As shown in Fig. 3(d–i), when the hCG was captured by anti-hCG-β Ab, additional MMSs functionalized with anti-hCG-α Ab will be added to the microchannel, where the MMSs will be bonded to the hCG on the fiber sensor surface as shown in Fig. 3(d–ii). Since the size of MMS is significantly larger than that of hCG, the MMSs attached to the fiber sensor surface will introduce significant changes of the effective RI and thickness to the fiber sensor, which will introduce significant wavelength shift of the sensor output, resulting in an improvement of sensor sensitivity.

The effect of adding anti-hCG-α Ab modified MMS is demonstrated in Fig. 5(a), where the MMSs used in the experiment are polystyrene microspheres encapsulated with $Fe_3O_4$ nanoparticles (PSMS, concentration 0.04 μg/mL and 300 nm diameter). As shown in Fig. 5(a), if there is no MMSs added to the system, the wavelength shift observed for 0.5 mIU/mL hCG is 0.62 nm (black squares), which can be amplified to 1.268 nm (red circles) by adding functionalised MMSs into the microchannel. This additional spectral shift is because of the bonding of anti-hCG-α Ab modified MMSs with the hCG sample captured on the fiber surface, as shown in Fig. 3(d–ii). The above hCG measurement includes a two-step process: (1) use anti-hCG-β Ab modified fiber sensor to detect hCG; (2) immerse the fiber sensor after step 1 into anti-hCG-α Ab modified MMSs liquid to enable binding between captured hCG and anti-hCG-α Ab modified MMSs. The above two-step process is compared with the direct hCG incubation process, where the anti-hCG-α Ab modified MMSs are directly mixed in the hCG sample and added into the microchannel to carry out the test. It can be observed from Fig. 5(a) that, direct incubation of hCG – MMS mixture introduces a wavelength shift of 1.271 nm (blue triangles) for 0.5 mIU/mL of hCG sample, which is similar to that of 1.268 nm for the two-step incubation process. Since the direct process is simpler than the two-step process, in the further experiments direct incubation is used for the test.

The effect of the MMSs' diameter on the sensor sensitivity is studied by using two types of MMSs (PSMS encapsulated with $Fe_3O_4$ nanoparticles) with 300 nm and 1 μm diameters, where anti-hCG-α Ab was attached onto the both types of the MMSs. In our experiments, the concentration of both the MMSs types was 0.4 μg/mL. Two identical STNCS sensors immobilised with 16 μg/mL of capture Ab were used to test the influence of the MMS-hCG samples, one for the 300 nm MMSs and one for the 1 μm MMSs. Fig. 5(b) shows the wavelength shift of the fiber sensor immersed into anti-hCG-α Ab modified MMSs (with 300 nm and 1 μm diameters), in different hCG concentrations. As shown in Fig. 5(b), there is a wavelength shift of 0.12, 0.57 and 0.95 nm for the MMSs with 300 nm diameters in 0.01, 0.05, 0.25 mIU/mL concentrations of hCG, respectively. When the particle size of the MMSs is increased to 1 μm diameter, the wavelength shift increases to 0.27, 1.27, and 2.17 nm for the same hCG concentrations of 0.01, 0.05, 0.25 mIU/mL, respectively, which is over 2 times higher sensitivity compared to that for the 300 nm MMSs. The maximum sensitivity achieved in this experiment is 27 nm/mIU/mL, by adding anti-hCG-α Ab modified MMSs with 1 μm diameter into the 0.01 mIU/mL hCG samples.

The sensitivity can be further improved by the enrichment of hCG samples. The enrichment process is called immunomagnetic separation, which is a conventional laboratory method to efficiently isolate the hCG in the urine sample or their dilution series in PBS (Herr et al., 2007). In our experiments, three hCG samples (2 mL each) with concentrations of 0.01, 0.05 and 0.25 mIU/mL, were incubated with anti-hCG-α Ab modified MMSs with diameters of 300 nm or 1 μm (0.4 μg/mL) in a tube for 10 min. The tube was then put on a magnetic separator for 2 min for the immunomagnetic separation, followed by the removal of supernatant. The MMSs captured with hCG, left in the tube were re-suspended in 400 μL of PBS and applied to the fiber sensor for measurements.

The effect of enrichment can be observed in Fig. 5(b). The three enriched hCG samples with MMSs of 300 nm diameter, showed a wavelength shift of 0.41, 1.26, and 2.44 nm for the hCG concentrations of 0.01, 0.05 and 0.25 mIU/mL, respectively. While the enriched hCG

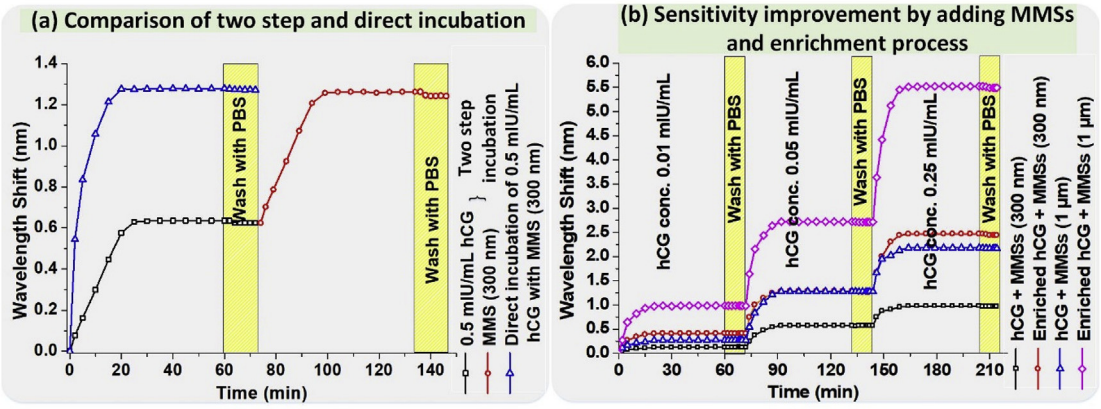


**Fig. 5.** (a) Comparison of the two step and direct incubation of functionalised STNCS fiber with hCG and MMSs and (b) Sensitivity improvement for 0.01, 0.05, and 0.25 mIU/mL of hCG obtained by adding MMSs with 300 nm and 1 μm diameters, and by enrichment process.

**Table 1**
Detected wavelength shift observed at different hCG concentrations using the three methods.

| hCG Concentration | Wavelength shift | | | | |
|---|---|---|---|---|---|
| (mIU/mL) | (nm) | | | | |
| | hCG only | hCG + MMS (300 nm) | Enriched hCG + MMS (300 nm) | hCG + MMS (1 μm) | Enriched hCG + MMS (1 μm) |
| 0.01 | – | 0.122 | 0.409 | 0.273 | 0.984 |
| 0.05 | 0.188 | 0.569 | 1.263 | 1.273 | 2.715 |
| 0.25 | 0.361 | 0.952 | 2.439 | 2.170 | 5.492 |

samples with MMSs of 1 μm diameter showed a wavelength shift of 0.98, 2.71, 5.49 nm for the same hCG concentrations of 0.01, 0.05 and 0.25 mIU/mL, respectively. The result shows that the sensitivity is further improved to 98 nm/mIU/mL by enriching the 0.01 mIU/mL hCG with MMSs of 1 μm diameter.

Table 1 summarizes the measured wavelength shift by the three methods explored above (using STNCS optical fiber sensor with (1) hCG only; (2) adding surface modified MMSs and (3) enrichment of hCG samples).

As shown in Table 1, when the concentration of hCG is 0.05 mIU/mL, there is 6.7 and 14 times improvement by adding MMSs of 1 μm diameter and enrichment of hCG samples, respectively, compared to that of the hCG only. When the hCG concentration is 0.01 mIU/mL, the fiber sensor cannot detect hCG directly. However, when the hCG is combined with surface modified MMSs, the sensor can detect hCG at the concentration as low as 0.01 mIU/mL, where 0.122 nm and 0.273 nm wavelength shifts are obtained for the MMSs with 300 nm and 1 μm diameters, respectively. The wavelength shift can be further improved to 0.984 nm when the hCG sample (combined with MMSs of 1 μm diameter) is enriched. Assuming the resolution of OSA is 0.01 nm, the LOD of the fiber sensor could be as low as 0.0001 mIU/mL, which is the lowest detection limit reported to date.

It is noted that the proposed sandwich immunoassays method has wide applications for other analytes detection, for example, it can be used for detection of other target proteins, microorganism (such as AFP, CEA, PSA, CA199) which have two antibodies. Similarly, sandwich hybridization assays which used for detecting target nucleic acids also can be realized using the proposed sensors with probe oligonucleotides modified onto their surfaces.

## 5. Conclusions

In this paper a novel sensitivity improvement method is proposed using functionalized MMSs to “amplify” the effect of target bio-chemical analytes. The method has been experimentally demonstrated using hCG as a detection target and STNCS optical fibre sensor with 8 μm waist diameter as a sensor platform. Experimentally we have achieved ultrahigh sensitivity hCG detection with LOD of 0.0001 mIU/mL, which is the highest reported so far. This research opens a new direction for sensitivity improvement based on existed fiber sensor and could be explored to applications require ultrahigh sensitivity detections such as earlier medical diagnostics. This method has relatively smaller measurement range compared to that without MMS. There is a tradeoff between sensitivity and dynamic range, which isn't clear at this stage. Further studies will be carried out using different “amplifier” particle materials (hence difference RI) and profiles (shape such as cylinder, sphere and dimensions) to investigate their effects on the sensor sensitivity and relationship between sensitivity and dynamic range.

## CRediT authorship contribution statement

**Rahul Kumar:** Formal analysis, Writing - original draft, Investigation. **Yuankui Leng:** Formal analysis, Writing - original draft, Investigation. **Bin Liu:** Formal analysis, Writing - original draft, Investigation. **Jun Zhou:** Formal analysis, Writing - review & editing. **Liyang Shao:** Supervision, Formal analysis, Writing - review & editing. **Jinhui Yuan:** Formal analysis, Writing - review & editing. **Xinyu Fan:** Supervision, Formal analysis, Writing - review & editing. **Shengpeng Wan:** Supervision, Formal analysis, Writing - review & editing. **Tao Wu:** Formal analysis, Writing - review & editing. **Juan Liu:** Formal analysis, Writing - review & editing. **Richard Binns:** Formal analysis, Writing - review & editing. **Yong Qing Fu:** Formal analysis, Writing - review & editing. **Wai Pang Ng:** Formal analysis, Writing - review & editing. **Gerald Farrell:** Formal analysis, Writing - review & editing. **Yuliya Semenova:** Formal analysis, Writing - review & editing. **Hengyi Xu:** Formal analysis, Writing - review & editing. **Yonghua Xiong:** Formal analysis, Writing - review & editing. **Xingdao He:** Supervision, Formal analysis, Writing - review & editing. **Qiang Wu:** Conceptualization, Supervision, Formal analysis, Writing - original draft, Methodology, Writing - review & editing.

## Acknowledgements

This work was support by Natural Science Foundation of Jiangxi Province under grant No. 20192ACB20031 and 20192ACBL21051; State Key Laboratory of Advanced Optical Communication Systems and Networks, Shanghai Jiao Tong University, China under grant No. 2018G2KF03003; the National Natural Science Foundation of China under grant No. 61465009.

## Appendix A. Supplementary data

Supplementary data to this article can be found online at https://doi.org/10.1016/j.bios.2019.111563.

## References

Berger, P., Sturgeon, C., 2014. Trends Endocrinol. Metab. 25 (12), 637–648.
Betancur-Ochoa, J.E., Minkovich, V.P., Montagut-Ferizzola, Y.J., 2017. J. Light. Technol. 35 (21), 4747–4751.
Douglas, J., Sharp, A., Chau, C., Head, J., Drake, T., Wheater, M., Geldart, T., Mead, G., Crabb, S.J., 2014. Br. J. Canc. 110 (7), 1759.
Fan, J., Wang, M., Wang, C., Cao, Y., 2017. Bioanalysis 9 (19), 1509–1529.
Hassan, M., Gonzalez, E., Hitchins, V., Ilev, I., 2016. Sens. Actuators B Chem. 231, 646–654.
Herr, F., Baal, N., Reisinger, K., Lorenz, A., McKinnon, T., Preissner, K.T., Zygmunt, M., 2007. Placenta 28, S85–S93.
Imamura, S., Miura, S., Ishiguro, M., Kikutani, M., Aikawa, T., Kitagawa, T., 1976. Rinsho Kagaku Shinpojumu 16, 28–32.
Keay, S.D., Vatish, M., Karteris, E., Hillhouse, E.W., Randeva, H.S., 2004. BJOG An Int. J. Obstet. Gynaecol. 111 (11), 1218–1228.
Liu, D., Mallik, A.K., Yuan, J., Yu, C., Farrell, G., Semenova, Y., Wu, Q., 2015. Opt. Lett. 40 (17), 4166–4169.
Liu, L.L., Marques, L., Correia, R., Morgan, S.P., Lee, S.W., Tighe, P., Fairclough, L., Korposh, S., 2018a. Sens. Actuators B Chem. 271, 24–32.
Liu, D., Kumar, R., Wei, F., Han, W., Mallik, A.K., Yuan, J., Wan, S., He, X., Kang, Z., Li, F., Yu, C., Farrell, G., Semenova, Y., Wu, Q., 2018b. Sens. Actuators B Chem. 271, 1–8.
Malhotra, S.S., Suman, P., Gupta, S.K., 2015. Sci. Rep. 5, 11210.
Mao, L., Yuan, R., Chai, Y., Zhuo, Y., Yang, X., 2010. Sens. Actuators B Chem. 149 (1), 226–232.
Mustapa, M.A., Bakar, M.H.A., Kamil, Y.M., Syahir, A., Mahdi, M.A., 2018. IEEE Sens. J. 18 (10), 4066–4072.
Noonan, F.P., Halliday, W.J., Morton, H., Clunie, G.J.A., 1979. Nature 278 (5705), 649–651.
Piliarik, M., Bocková, M., Homola, J., 2010. Biosens. Bioelectron. 26 (4), 1656–1661.

Pocius, K.D., Maurer, R., Fortin, J., Goldberg, A.B., Bartz, D., 2015. Contraception 91 (6), 503–506.
Pocius, K.D., Bartz, D., Maurer, R., Stenquist, A., Fortin, J., Goldberg, A.B., 2017. Contraception 95 (3), 263–268.
Santandreu, M., Alegret, S., Fabregas, E., 1999. Anal. Chim. Acta 396, 181–188.
Sepúlveda, B., Río, J Sánchez del, Moreno, M., Blanco, F.J., Mayora, K., Domínguez, C., Lechuga, L.M., 2006. J. Opt. A Pure Appl. Opt. 8 (7), S561–S566.
Shah, T., Srirajaskanthan, R., Bhogal, M., Toubanakis, C., Meyer, T., Noonan, A., Witney-Smith, C., Amin, T., Bhogal, P., Sivathasan, N., Warner, B., Hochhauser, D., Caplin, M.E., 2008. Br. J. Canc. 99 (1), 72.
Sheth, N., Saruiya, J., Ranadive, K., Sheth, A., 1974. Br. J. Canc. 30 (6), 566.
Soteropulos, C.E., Hunt, H.K., 2012. J. Vis. Exp.: J. Vis. Exp. 63, e3866.
Wang, B.T., Wang, Q., 2018. Opt. Commun. 426, 388–394.
Wang, J., Yuan, R., Chai, Y., Cao, S., Guan, S., Fu, P., Min, L., 2010. Biochem. Eng. J. 51 (3), 95–101.
Wu, Q., Semenova, Y., Wang, P., Farrell, G., 2011. Opt. Express 19 (9), 7937–7944.
Wysokiński, K., Budnicki, D., Fidelus, J., Szostkiewicz, Ł., Ostrowski, Ł., Murawski, M., Staniszewski, M., Staniszewska, M., Napierała, M., Nasiłowski, T., 2018. Biosens. Bioelectron. 114, 22–29.
Yan, X., Huang, Z., He, M., Liao, X., Zhang, C., Yin, G., Gu, J., 2012. Colloids Surf., B 89, 86–92.
Zhao, Y., Li, X.-g., Zhou, X., Zhang, Y.-n., 2016. Sens. Actuators B Chem. 231, 324–340.